JACS
JOURNAL OF THE AMERICAN CHEMICAL SOCIETY
Article
pubs.acs.org/JACS

Monothiol Glutaredoxins Can Bind Linear $[Fe_3S_4]^+$ and $[Fe_4S_4]^{2+}$ Clusters in Addition to $[Fe_2S_2]^{2+}$ Clusters: Spectroscopic Characterization and Functional Implications

Bo Zhang,[†,∥] Sibali Bandyopadhyay,[†,∥] Priyanka Shakamuri,[†] Sunil G. Naik,[‡] Boi Hanh Huynh,[‡] Jérémy Couturier,[§] Nicolas Rouhier,[§] and Michael K. Johnson*[,†]

[†]Department of Chemistry and Center for Metalloenzyme Studies, University of Georgia, Athens, Georgia 30602, United States
[‡]Department of Physics, Emory University, Atlanta, Georgia 30322, United States
[§]Interactions Arbres Microorganismes, Unité Mixte de Recherches 1136 Université de Lorraine-INRA, IFR 110, EFABA 54506 Vandoeuvre-lès-Nancy Cedex, France

Supporting Information

ABSTRACT: *Saccharomyces cerevisiae* mitochondrial glutaredoxin 5 (Grx5) is the archetypical member of a ubiquitous class of monothiol glutaredoxins with a strictly conserved CGFS active-site sequence that has been shown to function in biological $[Fe_2S_2]^{2+}$ cluster trafficking. In this work, we show that recombinant *S. cerevisiae* Grx5 purified aerobically, after prolonged exposure of the cell-free extract to air or after anaerobic reconstitution in the presence of glutathione, predominantly contains a linear $[Fe_3S_4]^+$ cluster. The excited-state electronic properties and ground-state electronic and vibrational properties of the linear $[Fe_3S_4]^+$ cluster have been characterized using UV−vis absorption/CD/MCD, EPR, Mössbauer, and resonance Raman spectroscopies. The results reveal a rhombic $S = 5/2$ linear $[Fe_3S_4]^+$ cluster with properties similar to those reported for synthetic linear $[Fe_3S_4]^+$ clusters and the linear $[Fe_3S_4]^+$ clusters in purple aconitase. Moreover, the results indicate that the Fe−S cluster content previously reported for many monothiol Grxs has been misinterpreted exclusively in terms of $[Fe_2S_2]^{2+}$ clusters, rather than linear $[Fe_3S_4]^+$ clusters or mixtures of linear $[Fe_3S_4]^+$ and $[Fe_2S_2]^{2+}$ clusters. In the absence of GSH, anaerobic reconstitution of Grx5 yields a dimeric form containing one $[Fe_4S_4]^{2+}$ cluster that is competent for *in vitro* activation of apo-aconitase, via intact cluster transfer. The ligation of the linear $[Fe_3S_4]^+$ and $[Fe_4S_4]^{2+}$ clusters in Grx5 has been assessed by spectroscopic, mutational, and analytical studies. Potential roles for monothiol Grx5 in scavenging and recycling linear $[Fe_3S_4]^+$ clusters released during protein unfolding under oxidative stress conditions and in maturation of $[Fe_4S_4]^{2+}$ cluster-containing proteins are discussed in light of these results.

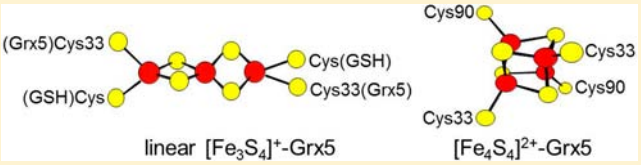

INTRODUCTION

Monothiol glutaredoxins with CGFS active sites (CGFS-Grxs) represent a unique class of glutaredoxins that exhibit negligible or low levels of thiol-disulfide oxidoreductase activity.[1−4] Rather both *in vivo* and *in vitro* studies of CGFS-Grxs indicate a role in trafficking $[Fe_2S_2]$ clusters in Fe−S cluster biogenesis.[5−10] This work demonstrates that CGFS-Grxs can also bind linear $[Fe_3S_4]^+$ and $[Fe_4S_4]^{2+}$ clusters, which raises the possibility of additional roles in scavenging and recycling $[Fe_3S_4]^+$ clusters released during protein unfolding under oxidative stress conditions and in the maturation of $[Fe_4S_4]^{2+}$ cluster-containing proteins.

The initial studies that revealed CGFS-Grxs as important components in Fe−S cluster biogenesis were carried out using *S. cerevisiae* mitochondrial Grx5 (*Sc* Grx5), a CGFS-Grx that has emerged as model protein for establishing the biological functions of this class of glutaredoxins.[6,10,11] A *grx5* deletion strain exhibited phenotypes that can be attributed to defective Fe−S cluster biogenesis, notably impaired activity of at least two mitochondrial Fe−S enzymes (aconitase and succinate dehydrogenase), mitochondrial iron accumulation, increased sensitivity to oxidative stress, and growth defects in minimal media.[5] In addition, radiolabeled ^{55}Fe immunoprecipitation studies revealed that depletion of *Sc* Grx5 results in Fe accumulation on Isu1, the primary scaffold protein for the assembly of Fe−S clusters by the mitochondrial iron-sulfur cluster assembly (ISC) machinery.[6] These *in vivo* results suggested that *Sc* Grx5 was required for dissociation of preassembled Fe−S cluster from Isu1 and/or the transfer of clusters from Isu1 to acceptor proteins. Further evidence linking CGFS-Grxs to Fe−S cluster biogenesis came from the observation that *Sc* Grx5 specifically interacts with at least two key components of the yeast mitochondrial ISC machinery, namely Isa1,[9] an Fe−S cluster carrier protein, and most recently Ssq1,[10] a molecular chaperone that facilitates release of Fe−S clusters from Isu1 in an ATP-dependent reaction. The involvement of CGFS-Grxs in Fe−S cluster biogenesis is also evolutionarily conserved, since homologues of *Sc* Grx5 from various species ranging from prokaryotes to eukaryotes have

Received: July 10, 2013
Published: September 13, 2013

dx.doi.org/10.1021/ja407059n | J. Am. Chem. Soc. 2013, 135, 15153−15164

been shown to have the ability to rescue the phenotype of the *grx5* deletion strain when targeted to *S. cerevisiae* mitochondria.[7,12,13]

Site-directed mutagenesis studies on *Sc* Grx5 revealed that the CGFS cysteine residue is essential for its biological function, since mutation of this cysteine results in the same phenotype as observed in the *grx5* deletion strain.[14] In addition, both spectroscopic and structural studies of a variety of other reconstituted or as-purified prokaryotic and eukaryotic CGFS-Grxs have shown that the active-site cysteine along with the cysteine of two glutathione (GSH) molecules are required to coordinate a $[Fe_2S_2]^{2+}$ cluster at the subunit interface of the homodimer.[2,7,15] The $[Fe_2S_2]^{2+}$ cluster in homodimeric CGFS-Grxs have a homogeneous $S = 0$ ground state that results from antiferromagnetic coupling of the two high spin $S = 5/2$ ferric irons.[7] However, the $[Fe_2S_2]^{2+}$ clusters in CGFS-Grxs homodimers are unlikely to be redox active *in vivo* since the cluster is both oxidatively and reductively labile.

Thus far, there is only limited information regarding the ability of *Sc* Grx5 to incorporate an Fe−S cluster. Initially, Picciocchi and co-workers reported purification of a cluster-bound form of recombinant *Sc* Grx5 and the type of the cluster was interpreted as $[Fe_2S_2]$ cluster on the basis of UV−vis absorption data alone.[16] More recently, it has been demonstrated that *Sc* Grx5 is able to bind a Fe−S cluster *in vivo*, albeit at low levels of cluster incorporation.[10] However, the nature of the bound Fe−S cluster in *Sc* Grx5 was not unequivocally identified in either study. Using the combination of UV−vis absorption, circular dichroism (CD), and variable-temperature magnetic circular dichroism (VTMCD), electron paramagnetic resonance (EPR), Mössbauer and resonance Raman spectroscopies, we demonstrate here that anaerobic cluster reconstitution on recombinant *Sc* Grx5 or prolonged exposure of the cell-free extract containing overexpressed *Sc* Grx5 to air prior to aerobic purification, primarily results in the formation of a linear $[Fe_3S_4]^{+}$ cluster-bound form in the presence of GSH. In contrast anaerobic reconstitution in the absence of GSH results in a homogeneous $[Fe_4S_4]^{2+}$ cluster-bound from of *Sc* Grx5. The ligation of the assembled Fe−S clusters and the significance of the presence of linear $[Fe_3S_4]^{+}$ and $[Fe_4S_4]^{2+}$ clusters in *S. cerevisiae* Grx5 are examined and discussed in light of these new results.

MATERIALS AND METHODS

Plasmid Constructions. The sequence coding for the mature form of *S. cerevisiae* Grx5 devoid of the first 29 amino acids, corresponding to the mitochondrial targeting sequence, was cloned into the pET3d vector between NcoI and *Bam*HI restriction sites using the forward and reverse primers described in Table S1. Owing to the use of NcoI for cloning, an alanine codon was added to keep the sequence in frame. The C90S variant, in which the cysteine at position 90 was substituted by a serine residue, was also cloned by PCR into pET3d using two complementary primers (see Table S1). All plasmids were verified by sequencing.

Protein Expression and Purification. Recombinant *Sc* Grx5 was heterologously expressed in the *Escherichia coli* BL21(DE3) strain in the presence of the pSBET plasmid. Cells harboring the Grx5 plasmid were cultivated at 37 °C in LB media supplemented with ampicillin (100 μg/mL) and kanamycin (30 μg/mL). Protein expression was induced with isopropyl-1-thio-β-D-galactopyranoside (IPTG) to a final concentration of 100 μg/mL when OD_{600} was between 0.4 and 0.8. The culture was then further cultivated at 34 °C for 4 h and harvested by centrifugation and stored at −80 °C until further use. For aerobic purification, cells expressing recombinant *Sc* Grx5 were thawed and resuspended in 100 mM Tris-HCl, pH 7.8 buffer containing 1 mM GSH (buffer A) with addition of 10 μg/mL phenylmethylsulfonyl fluoride (PMSF), 15 μg/mL DNase and 5×10^{-3} μg/mL RNase. Cells were disrupted by intermittent sonication on ice and centrifuged at 17 000 rpm at 4 °C for 1 h to remove the cell debris. The cell-free extract was then precipitated with 40% of ammonium sulfate and pelleted by centrifugation. The resulting pellet was resuspended in minimal volume of buffer A, loaded onto a phenyl-sepharose High-Performance Fast-Flow (Pharmacia) column, previously equilibrated with 100 mM Tris-HCl, pH 7.8, containing 1 mM GSH and 1 M ammonium sulfate (buffer B) and eluted using a decreasing linear gradient from 1 to 0 M ammonium sulfate. The purest fractions judged by SDS-PAGE analysis were combined and concentrated down to ∼3 mL using YM10 membrane and then applied to a HiTrap^{M} Q-HP anion-exchange column (GE Healthcare) previously equilibrated with buffer A, and the elution was achieved with an increasing linear gradient from 0 to 1 M NaCl. The purest fractions containing apo *Sc* Grx5, as judged by SDS-PAGE analysis, were pooled and dialyzed into 100 mM Tris-HCl, pH 7.8 buffer by Amicon ultrafiltration using a YM10 membrane and stored in liquid nitrogen. Anaerobic purification of *Sc* Grx5 was carried out in a glovebox under an argon atmosphere (O_2 < 2 ppm) using the same protocol described above, except that lysis of the cells containing overexpressed *Sc* Grx5 was achieved by incubation with Ready-Lyse (Epicentre).

The *Sc* Grx5 C90S mutant was expressed in the *E. coli* BL21(DE3) strain in the presence of the pSBET plasmid and purified following the procedures previously described for *Arabidopsis* chloroplastic glutaredoxin C5.[17] Briefly, after cell lysis, the protein fraction was precipitated from the cell-free extract between 40 and 80% ammonium sulfate saturation, and *Sc* Grx5 C90S was purified aerobically using an ACA44 gel filtration column and followed by a DEAE ion exchange column. The purified proteins were finally stored in Tris buffer (30 mM Tris-HCl, pH 8.0) in liquid nitrogen.

***In Vitro* Reconstitution of Sc Grx5 in the Presence of GSH.** Prior to use, as-purified apo *Sc* Grx5 protein samples were incubated with 40 mM tris(2-carboxyethyl)phosphine (TCEP) under anaerobic conditions to reduce disulfides, followed by anaerobic removal of TCEP by buffer exchange using Amicon ultrafiltration with a YM10 membrane. Reconstitution was achieved by incubation of TCEP-pretreated *Sc* Grx5 with 20-fold excess of ferrous ammonium sulfate, 20-fold excess of L-cysteine, catalytic amount of NifS, and 3 mM of GSH under strictly anaerobic conditions (<2 ppm O_2) at room temperature for 2.5 h. Excess reagents were then removed by passing the reconstitution mixture through a Hi-Trap Q-Sepharose column (GE Healthcare) with an increasing linear gradient from 0 to 1 M NaCl. The colored fractions eluted were pooled and concentrated using a YM10 membrane. Samples for resonance Raman isotopic labeling studies were reconstituted with Na_2S (natural abundance S) or $Na_2{}^{34}S$ (>95% ^{34}S enrichment) in place of L-cysteine and NifS. ^{57}Fe-enriched ferrous ammonium sulfate (>95% ^{57}Fe enrichment) was used in place of natural abundance Fe for the preparation of Mössbauer samples. The same reconstitution procedure described above was used for the *Sc* Grx5 C90S mutant.

dx.doi.org/10.1021/ja407059n | J. Am. Chem. Soc. 2013, 135, 15153−15164

***In Vitro* Reconstitution of Sc Grx5 in the Absence of GSH.** TCEP-pretreated *Sc* Grx5 was incubated with 20-fold excess of ferrous ammonium sulfate, 20-fold excess of L-cysteine, and a catalytic amount of NifS under strictly anaerobic conditions (<2 ppm O_2), both in the presence and absence of 5 mM DTT. The same procedure for removing of excess reagents was performed as that described above. Mössbauer samples were prepared with ^{57}Fe-enriched ferrous ammonium sulfate (>95% enrichment). The same reconstitution procedure was used for the *Sc* Grx5 C90S mutant.

Analytical and Spectroscopic Analyses. Protein concentrations were determined using the *DC* Protein Assay (Bio-Rad) with bovine serum albumin as the standard. Iron concentrations were determined colorimetrically using method described by Fish after digestion of protein samples in $KMnO_4$/HCl.[18] For GSH measurements, apo and reconstituted *Sc* Grx5 samples were denatured and precipitated with 1% 5-sulfosalicylic acid, and the concentration of GSH in the supernatant was determined using the 5′,5′-dithiobis(2-nitrobenzoic acid)-GSSG reductase cycling assay as previously described.[19,20] Mass spectrometry analysis was carried out by the University of Georgia Proteomic and Mass Spectrometry Core Facility. All samples for spectroscopic studies were prepared in a Vacuum Atmospheres glovebox under argon atmosphere (O_2 < 2 ppm). UV−vis absorption spectra were recorded in sealed 1 mm quartz cuvettes at room temperature using a Shimadzu UV-3101 PC scanning spectrophotometer. Resonance Raman samples were in the form of 20 μL frozen droplet mounted on the coldfinger of an Air Products Displex Model CSA-202E closed cycle refrigerator, and resonance Raman spectra were recorded as previously described, using an Instrument SA Ramanor U1000 scanning spectrometer coupled with a Coherent Sabre argon or krypton ion laser.[21] X-band (~9.6 GHz) EPR spectra were recorded using a ESP-300D spectrometer (Bruker, Billerica, MA) equipped with a dual-mode ER-4116 cavity and an ESR 900 helium flow cryostat (Oxford Instruments, Concord, MA). Room temperature circular dichroism (CD) spectra were recorded in sealed 1 mm quartz cuvettes using a Jasco J-715 spectropolarimeter. Variable-temperature magnetic circular dichroism (VTMCD) spectra were recorded on samples containing 50% (v/v) ethylene glycol using the same spectropolarimeter mated to an Oxford Instruments Spectromag 4000 (0−7 T) split-coil superconducting magnet (1.5−300 K). Variable-temperature, variable-magnetic field (VTVH) MCD saturation magnetization data were measured by recording MCD intensity at a fixed wavelength and temperature for magnetic fields between 0 and 6 T and were analyzed using software provided by Professor Edward Solomon.[22] Mössbauer spectra of ^{57}Fe-enriched samples were recorded using the previously described instrumentation and analyzed using WMOSS software (Web Research).[23]

Activation of Apo-Aconitase Using $[Fe_4S_4]^{2+}$ Cluster-Bound Sc Grx5. Purification of recombinant *Azotobacter vinelandii* aconitase with a polyhistidine tag was carried out as previously described.[24] The apo form of aconitase was obtained by incubation of as-purified aconitase with EDTA and potassium ferricyanide using the method described by Kennedy and Beinert.[25] Activation mixtures contained 100 mM Tris-HCl (pH 7.8), 1 mM DTT, 4 μM of apo acontiase and 12 μM of $[Fe_4S_4]^{2+}$ cluster-bound *Sc* Grx5. The molar concentration corresponds to the concentration of the $[Fe_4S_4]^{2+}$ cluster calculated by using the molar absorption coefficient of ε_{400} = 16.9 mM^{-1} cm^{-1} per $[Fe_4S_4]^{2+}$ cluster. Activation mixtures were incubated at room temperature under strictly anaerobic conditions, and 10 μL aliquots of sample were taken at different time points and assayed for aconitase activity as previously described.[24,26] Briefly, the activity of aconitase was measured spectrophotometrically at 240 nm at room temperature by following the formation of *cis*-aconitate from citrate or isocitrate, using a molar absorption coefficient ε_{240} of 3400 mM^{-1} cm^{-1} for *cis*-aconitate.[27] Anaerobically reconstituted samples of *A. vinelandii* aconitase containing one $[Fe_4S_4]^{2+}$ cluster per monomer exhibited maximal specific activity (corresponding to 100% activity) of 25 units/mg using citrate and 79 units/mg using isocitrate.[24] The time course of holo aconitase formation at room temperature was analyzed by fitting to second-order kinetics, based on the initial concentrations of apo aconitase and $[Fe_4S_4]^{2+}$ clusters on *Sc* Grx5, using the Chemical Kinetics Simulator software package (IBM).

RESULTS

Characterization of Sc Grx5 as Purified. The mature form of *S. cerevisiae* Grx5 lacking the mitochondrial targeting sequence was heterologously expressed in *E. coli* and purified to homogeneity. Due to the requirement of GSH to coordinate the $[Fe_2S_2]^{2+}$ clusters in CGFS-type Grxs, 1 mM of GSH was added throughout the purification process.[2,15] The molecular mass of the purified *Sc* Grx5 sample was determined by electrospray mass spectrometry to be 13418 Da, in agreement with the predicted monomer molecular mass based on the expressed construct (Figure S1). Mass analysis of *Sc* Grx5 also identified two additional peaks at 13723 and 14028 Da, which correspond to the addition of one and two GSH molecules, respectively. This observed glutathiolation of *Sc* Grx5 is consistent with previously reported biochemical characterization results.[1] Samples of *Sc* Grx5 purified aerobically immediately after breaking open the cells were exclusively in the apo-form devoid of any type of bound Fe−S cluster, as judged by the absence of bands associated with the characteristic S-to-Fe(III) charge-transfer transitions in the visible absorption spectrum. Moreover, the absence of Fe−S clusters in as-purified *Sc* Grx5 was not due to oxygen exposure during purification, as purification carried out under strictly anaerobic conditions inside the glovebox also did not result in a Fe−S cluster-bound form of *Sc* Grx5.

In Vitro Reconstitution of Fe−S Clusters on Sc Grx5 in the Presence of GSH. In order to address the ability of *S. cerevisiae* Grx5 to incorporate Fe−S clusters, anaerobic cysteine desulfurase-mediated cluster reconstitution experiments were carried out in the presence of 3 mM of GSH, since all of the spectroscopically and crystallographically characterized $[Fe_2S_2]^{2+}$ clusters in other CGFS-Grxs are ligated by GSH molecules in addition to the Grx active-site cysteine residues.[2,7,15,28,29] After removal of excess reagents using chromatography, a cluster-loaded form of *Sc* Grx5 with strong absorption in the visible region was obtained (Figure 1A, blue spectrum). The $[Fe_2S_2]^{2+}$ centers in CGFS-Grxs all exhibit very similar UV−vis absorption and CD spectra (see Figure 1A black spectra)[7,28,29] that are quite distinct to those observed for the cluster-bound *Sc* Grx5. Notably, the UV−vis absorption spectrum of the Fe−S cluster in the reconstituted *Sc* Grx5 exhibits two additional pronounced bands at 566 and 513 nm, and the dominant band at 400 nm is blue-shifted by ~10 nm compared to the equivalent band of the $[Fe_2S_2]^{2+}$ clusters.

dx.doi.org/10.1021/ja407059n | J. Am. Chem. Soc. 2013, 135, 15153−15164

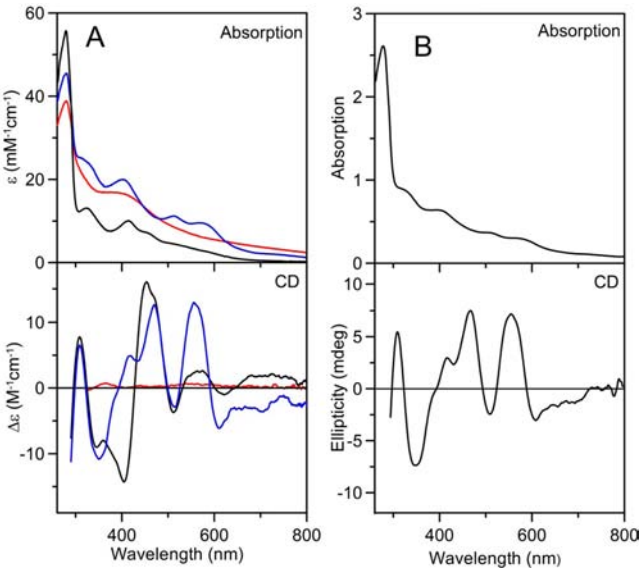

Figure 1. (A) Comparison of the linear $[Fe_3S_4]^+$ cluster-bound (blue line) and $[Fe_4S_4]^{2+}$ cluster-bound (red line) forms of reconstituted *Sc* Grx5 and the $[Fe_2S_2]^{2+}$ cluster-bound reconstituted *Sc* Grx3 homodimer (black line). Spectra were recorded under anaerobic conditions in sealed 0.1 cm cuvettes in 100 mM Tris-HCl buffer with 1 mM GSH at pH 7.8 for linear $[Fe_3S_4]$-Grx5, in 100 mM Tris-HCl buffer with 1 mM DTT at pH 7.8 for $[Fe_4S_4]$-Grx5 and in 100 mM Tris-HCl buffer with 250 mM NaCl at pH 7.8 for $[Fe_2S_2]$-Grx3. The ε and $\Delta\varepsilon$ values are based on the *Sc* Grx5 and *Sc* Grx3 protein homodimer concentrations. The spectra of *Sc* Grx3 are taken from ref 29. (B) UV−vis absorption and CD evidence for linear $[Fe_3S_4]^+$ clusters in recombinant *S. cerevisiae* Grx5 partially purified after being exposed to air at 4 °C for 15 days as the supernatant of a 40% ammonium sulfate cut of the cell-free extract (see text for details).

Furthermore, the CD spectra of the cluster-bound *Sc* Grx5 and the $[Fe_2S_2]^{2+}$ cluster-bound *Sc* Grx3 exhibit major differences with the former exhibiting an intense positive band at 580 nm and a small positive feature at 418 nm that is not observed in any $[Fe_2S_2]^{2+}$ cluster-containing homodimeric CGFS-Grxs (Figure 1A). Surprisingly, the absorption features of the cluster-bound *Sc* Grx5 in the visible range are strikingly similar to those previously reported for the linear $[Fe_3S_4]^+$ clusters in synthetic complexes and in alkaline (purple) aconitase.[30,31] On the basis of the theoretical and experimental ε_{280} values for the monomeric apo protein (8.6 $mM^{-1}cm^{-1}$), the ε_{280} and ε_{403} values for the linear $[Fe_3S_4]^+$ cluster in homodimeric *Sc* Grx5 are estimated to be 28.4 and 20.0 $mM^{-1}cm^{-1}$, respectively, for a sample with a maximal A_{403}/A_{280} value of 0.44. These extinction coefficient values are similar to those established for synthetic and biological linear $[3Fe\text{-}4S]^+$ clusters ($\varepsilon_{280} \sim 30$ $mM^{-1}cm^{-1}$ and $\varepsilon_{400} \sim 20$ $mM^{-1}cm^{-1}$),[30,31] indicating one linear $[3Fe\text{-}4S]^+$ cluster per *Sc* Grx5 homodimer. Moreover, protein and Fe analysis of a sample in which ∼70% of *Sc* Grx5 was cluster-loaded ($A_{403}/A_{280} = 0.37$ and $\varepsilon_{403} = 14.0$ $mM^{-1}cm^{-1}$), indicated 1.1 ± 0.1 Fe per Grx5 monomer. Taking into account the Fe−S cluster occupancy of this sample, this indicates 1.6 ± 0.2 Fe per Grx5 monomer for fully cluster-loaded *Sc* Grx5, which is also indicative of one linear $[Fe_3S_4]^+$ cluster per *Sc* Grx5 homodimer.

As indicated above, Fe−S cluster-bound forms of recombinant *Sc* Grx5 were not observed in samples purified immediately after breaking open the *E. coli* cells under either aerobic or anaerobic conditions. However, it was noted that the almost colorless supernatant of an aerobic 40% ammonium sulfate cut of the cell-free extract developed a brown color after being left at 4 °C for 15 days. Following partial purification with a phenyl sepharose column, the sample exhibited the characteristic UV−vis absorption and CD spectra *Sc* Grx5 containing a linear $[Fe_3S_4]^+$ cluster, see Figure 1B. Moreover, comparison of the UV−vis absorption and CD spectra of the *E. coli* cell-free extract taken immediately after aerobic sonication and after leaving at 4 °C for 24 h in air, clearly demonstrates the formation of linear $[Fe_3S_4]^+$ clusters on recombinant *Sc* Grx5, see Figure S2. The implication of both experiments is that *Sc* Grx5 is capable of either scavenging linear $[Fe_3S_4]^+$ clusters that are generated by Fe−S proteins denatured under oxidative stress conditions or reconstituting linear $[Fe_3S_4]^+$ clusters from the iron and sulfide produced by Fe−S cluster degradation under oxidative stress conditions.

More definitive and quantitative assessment of the type of Fe−S cluster(s) present in *Sc* Grx5 was provided by Mössbauer studies of a sample reconstituted with ^{57}Fe. Figure 2A shows a 4.2 K Mössbauer spectrum (black vertical bars) of *Sc* Grx5 reconstituted in the presence of 3 mM GSH, recorded in a weak magnetic field of 50 mT parallel to the γ-radiation. Four components are discernible in this complex spectrum. The major component, which accounts for 72% of total ^{57}Fe absorption, exhibits paramagnetic hyperfine structure (shown in orange). This component is identified as arising from a linear $[Fe_3S_4]^+$ cluster based on analysis of data collected at different applied magnetic fields (*vide infra*). The remaining three components contained in this sample arise from a $S = 0$ $[Fe_2S_2]^{2+}$ cluster that accounts for 11% of the total ^{57}Fe absorption (shown in red), a $S = 0$ $[Fe_4S_4]^{2+}$ cluster accounting for 6% of the total ^{57}Fe absorption (shown in blue), and a mononuclear $S = 2$ Fe^{2+} species, estimated to contribute for 11% of the total ^{57}Fe absorption (shown in green). The solid black line overlaid on the experimental spectrum in Figure 2A is the composite spectrum that includes all four components. The agreement between the simulated spectrum and the experimental data supports the above assessment of the composition of Fe species in the sample.

Removal of the contributions from the minor components ($[Fe_2S_2]^{2+}$ and $[Fe_4S_4]^{2+}$ clusters and Fe^{2+} species) reveals the experimental spectrum arising solely from the linear $[Fe_3S_4]^+$ cluster (black vertical-bar spectrum in Figure 2B). To better characterize the linear $[Fe_3S_4]^+$ cluster in *Sc* Grx5, additional Mössbauer spectra were recorded at 4.2 K with 4 and 8 T parallel fields and the contributions from the $[Fe_2S_2]^{2+}$ and $[Fe_4S_4]^{2+}$ clusters and Fe^{2+} species were again removed from the raw data (black spectra in Figure 2C,D, respectively). The Mössbauer spectra of the linear $[Fe_3S_4]^+$ cluster in *Sc* Grx5 with 50 mT and 4 and 8 T are analogous to the Mössbauer spectra of the linear $[Fe_3S_4]^+$ cluster in aconitase[31] and can be decomposed into three equal intensity subcomponents, each arising from a high-spin ($S = 5/2$) ferric site in a tetrahedral environment of sulfur atoms. The field-dependence of the magnetic hyperfine splitting pattern further demonstrates that the three Fe sites are spin−spin coupled to form a total spin $S = 5/2$ ground state with the spin of the central Fe (site 3) antiparallel to both terminal Fe sites (sites 1 and 2), consistent with the spin coupling model established for the linear $[Fe_3S_4]^+$ cluster in aconitase and the synthetic complexes.[31,32]

The observed magnetic hyperfine splitting of the Mössbauer spectrum of a Fe site is directly proportional to the magnitude of the effective field at the Fe site, B_{eff}, which is the sum of the

dx.doi.org/10.1021/ja407059n | J. Am. Chem. Soc. 2013, 135, 15153−15164

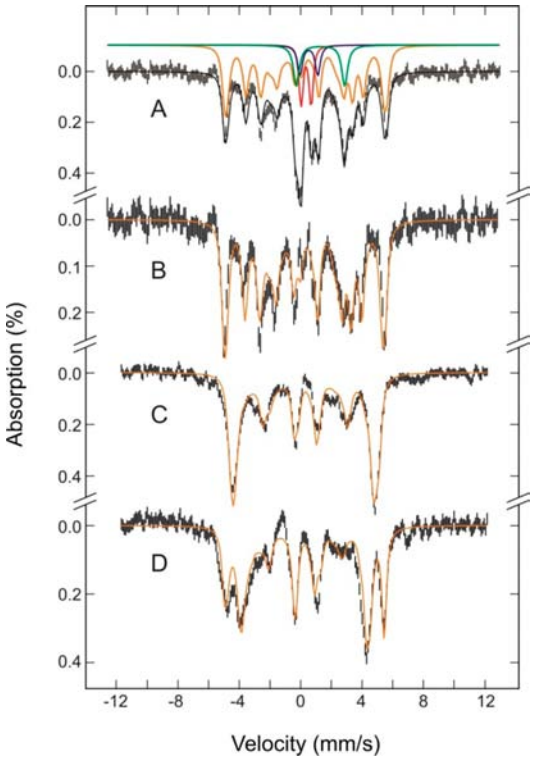

Figure 2. Mössbauer evidence for linear $[Fe_3S_4]^+$ clusters in *Sc* Grx5 reconstituted with ^{57}Fe in the presence of GSH. The sample was ~4 mM in ^{57}Fe and was in 100 mM Tris-HCl buffer, pH 7.8 with 1 mM GSH. The spectra (black vertical bars) were recorded at 4.2 K with a weak field (50 mT in A, B) and high fields (4T in C and 8T in D) applied parallel to the γ-radiation. The solid orange lines in all spectra are theoretical spectra for the linear $[Fe_3S_4]^+$ cluster in *S. cerevisiae* Grx5 computed with the parameters listed in Table 1. The solid black line overlaid on the experimental spectrum in A is the composite spectrum generated by adding the simulated spectra of the linear $[Fe_3S_4]^+$ cluster (scaled to 72% of the total iron absorption) and $[Fe_2S_2]^{2+}$ cluster (11% of the total iron absorption, red line), $[Fe_4S_4]^{2+}$ cluster (6% of the total iron absorption, blue line) and adventitiously bound Fe^{2+} (11% of the total iron absorption, green line). The parameters used to simulate the $[Fe_2S_2]^{2+}$ cluster are the same as those used to simulate the $[Fe_2S_2]^{2+}$ cluster in poplar GrxS14.[7] The parameters used to simulate the $[Fe_4S_4]^{2+}$ cluster are the same as those used to simulate the $[Fe_4S_4]^{2+}$ cluster in *Sc* Grx5 reconstituted in the presence of DTT, see text for details. The spectra in B, C, and D were obtained by subtracting the contribution of the $[Fe_2S_2]^{2+}$ and $[Fe_4S_4]^{2+}$ clusters and the adventitiously bound Fe^{2+} species from the raw spectra recorded at 50 mT, 4 and 8 T, respectively.

internal magnetic field at that Fe site, $\mathbf{B}_{int}$, and the applied field, B, and can be written as $|\mathbf{B}_{eff}| = |\mathbf{B}_{int} + B|$. The internal magnetic field can be expressed as $\mathbf{B}_{int} = -\tilde{\mathbf{A}}\cdot\langle\mathbf{S}\rangle/g_n\beta_n$, where $\langle\mathbf{S}\rangle$ is the expectation value of the electronic spin of the occupied state and $\tilde{\mathbf{A}}$ is the magnetic hyperfine coupling tensor. At low temperature (4.2 K) in a strong applied field (B > 2 T), only the lowest spin-down state ($\langle\mathbf{S}\rangle$ < 0) is appreciably occupied. Thus, depending on the sign of $\tilde{\mathbf{A}}$, the effective field, and hence the magnetic hyperfine splitting, will either increase or decrease with an increasing applied field. For a mononuclear high-spin ferric site, $\tilde{\mathbf{A}}$ is negative and relatively isotropic and may be approximated by a negative constant a. Consequently, the magnetic splitting for a monomeric high-spin ferric site is always decreasing with increasing strong applied field. The only situation for a high-spin ferric site to exhibit increasing magnetic splitting with increasing applied field will be for the site to participate in a strongly spin−spin coupled system where its intrinsic spin is oriented antiparallel to the system spin due to spin−spin interaction. According to the spin-coupling model established for the S = 5/2 linear $[Fe_3S_4]^+$ cluster,[31,32] the observed magnetic hyperfine constants for the three ferric sites (A_1, A_2, and A_3) are related to their corresponding intrinsic magnetic hyperfine constants (a_1, a_2, and a_3) as

$$A_1 = \frac{6}{7}a_1, \quad A_2 = \frac{6}{7}a_2, \quad \text{and} \quad A_3 = -\frac{5}{7}a_3 \tag{1}$$

Tetrahedral sulfur coordinated high-spin ferric sites exhibit small quadrupole splitting ($|\Delta E_Q|$ ~0.5− 0.7 mm/s) and show a narrow range of $a/g_n\beta_n$ values between −16 to −14 T. Thus, the model suggests the following characteristics for the Mössbauer spectrum of a linear $[Fe_3S_4]^+$ cluster. It would be composed of three magnetic hyperfine split components of equal intensity. Two of the components, corresponding to the terminal Fe sites 1 and 2, would have negative magnetic hyperfine coupling constants, $A_1/g_n\beta_n$ and $A_2/g_n\beta_n$, of comparable values around −13 T. They are, therefore, similar and unresolved. The magnetic hyperfine splittings of these two components would be decreasing with increasing applied field due to the negative A_1 and A_2 values. The remaining component, corresponding to the central Fe site 3, is unique with a positive magnetic hyperfine coupling constant of smaller magnitude, about +10 T. Its magnetic hyperfine splitting, therefore, would increase with increasing applied field. All these characteristics are clearly detected in the Mössbauer spectra of the linear $[Fe_3S_4]^+$ cluster in *Sc* Grx5 (Figure 2B−D).

In accord with the EPR studies (*vide infra*), the electronic state of the $[Fe_3S_4]^+$ cluster is interpreted with $D \sim 2.0$ cm^{-1} and E/D = 0.31. At 4.2 K with a weak field of 50 mT, only the lowest Kramers doublet is occupied. This doublet is magnetically uniaxial, with g_y = 9.6, g_x, g_z < 1. Thus, to a good approximation, $\langle\mathbf{S}\rangle_x \sim \langle\mathbf{S}\rangle_z \sim 0$, and $\langle\mathbf{S}\rangle_y \sim \pm g_y/4$, which is close to the spin saturation values of the formal $M_s = \pm$ 5/2 doublet. The observed spectrum (Figure 2B) displays well-resolved and sharp absorption peaks and can be explained as the sum of two magnetically split spectral components with an intensity ratio of 2 to 1. As expected from the linear $[Fe_3S_4]^+$ cluster model (*vide supra*), the intense component, arising from the two terminal Fe sites, exhibits a large magnetic splitting as shown by the two outermost peaks at −5 and +5.5 mm/s. The

Table 1. Mössbauer Parameters for the Linear $[Fe_3S_4]^+$ Cluster in *Sc* Grx5[a]

Fe site	$A_{xx}/g_n\beta_n$ (T)	$A_{yy}/g_n\beta_n$ (T)	$A_{zz}/g_n\beta_n$ (T)	ΔE_Q (mm/s)	η	eQV_{yy} (mm/s)	δ (mm/s)
1	−13.0	−13.7	−13.7	−0.64	−1.2	−0.05	0.28
2	−12.0	−13.2	−10.0	−0.73	−1.3	−0.10	0.28
3	+10.0	+9.9	+10.5	+0.57	+0.5	−0.40	0.38

[a]The Mössbauer data were analyzed for an S = 5/2 ground state with E/D = 0.31, D = 2.0 cm^{-1}, $g_x = g_y = g_z$ = 2.0.[31] The simulated Mössbauer spectra were generated with equal intensity from each of the three iron sites.

dx.doi.org/10.1021/ja407059n | J. Am. Chem. Soc. 2013, 135, 15153−15164

weak component, arising from the central Fe site, exhibits a smaller magnetic splitting as shown by the two resonance peaks at −4 and +4 mm/s. These magnetic hyperfine splittings indicate effective magnetic fields along the g_y axis of ∼32 T for the terminal Fe sites and ∼24 T for the central Fe site, providing magnitudes of the magnetic hyperfine coupling values (∼13 and 10 T, respectively) that are in good agreement with those predicted by the model. The well-resolved pattern of this spectrum also allowed us to have an accurate determination of the isomer shifts and components of the electric field gradients along the g_y axis for all three Fe sites (Table 1, last two columns). These parameters compare very well with those reported for the linear $[Fe_3S_4]^+$ cluster in aconitase.[31] To determine the signs of the $\tilde{\mathbf{A}}$ tensors and remaining parameters, we analyzed the strong-field spectra (Figure 2C,D).

The Mössbauer spectrum of the linear $[Fe_3S_4]^+$ cluster in *Sc* Grx5 at 4 T (Figure 2C) displays a much simplified splitting pattern with stronger intensity in comparison with that at 50 mT (Figure 2B). The magnetic splitting of the 4 T spectrum is in between those of the two subcomponents observed at 50 mT. In other words, the effect of the 4 T applied field is to decrease the magnetic splitting of the intense component and increase the magnetic splitting of the weak component so that both components overlap. At 8 T, the intense component shows a further decrease in its magnetic splitting and becomes separated from the weak component. The weak component continues to increase its magnetic splitting and appears as the component with the two outermost absorption peaks. Thus, the strong-field spectra demonstrate unambiguously that the magnetic hyperfine tensors for sites 1 and 2 (the intense component) are negative, while that of site 3 (the weak component) is positive, consistent with the prediction made by the established spin coupling model. To analyze the Mössbauer spectra of the linear $[Fe_3S_4]^+$ cluster in *Sc* Grx5 (Figure 2B−D) in detail, we employ the spin Hamiltonian formulism developed by Kennedy et al.[31] for the linear $[Fe_3S_4]^+$ cluster in aconitase. All spectra are simulated to a good approximation using the parameters listed in Table 1, shown as orange lines overlaying the experimental spectra in Figure 2A−D. The theoretical simulations are computed with equal intensity for each Fe site, and a rhombic $S = 5/2$ ground state with $E/D = 0.31$ and $D = 2.0$ cm^{-1}, i.e., analogous spin Hamiltonian parameters to those used in simulating the Mössbauer spectrum of the linear $[Fe_3S_4]^+$ cluster in aconitase.[31]

The linear $[Fe_3S_4]^+$ cluster in *Sc* Grx5 was also investigated by EPR spectroscopy to further assess the electronic ground-state properties. On the basis of the parallel Mössbauer studies on the same sample, ∼30% of the cluster-bound *Sc* Grx5 sample was shown to contain $[Fe_2S_2]^{2+}$ and $[Fe_4S_4]^{2+}$ clusters and a mononuclear high-spin ($S = 2$) ferrous species. However, both $[Fe_2S_2]^{2+}$ and $[Fe_4S_4]^{2+}$ clusters have diamagnetic ground states and the high-spin $S = 2$ ferrous species does not exhibit an observable EPR signal using perpendicular or parallel mode X-band EPR. Therefore, the presence of these additional components does not interfere with the EPR characterization of the linear $[Fe_3S_4]^+$ cluster in *Sc* Grx5. The X-band EPR spectra of the linear $[Fe_3S_4]^+$ cluster-containing form of *Sc* Grx5 recorded at 4.3, 10, and 20 K display a sharp derivative-shaped resonance at $g = 4.3$ and broad absorption-shaped low-field features centered at $g = 8.7$ and 5.3 (Figure 3). The $g = 4.3$ component is consistent with the $S = 5/2$ spin Hamiltonian used to interpret the Mössbauer (*vide supra*) and MCD saturation magnetization data (*vide infra*), i.e., $E/D = 0.31$ and

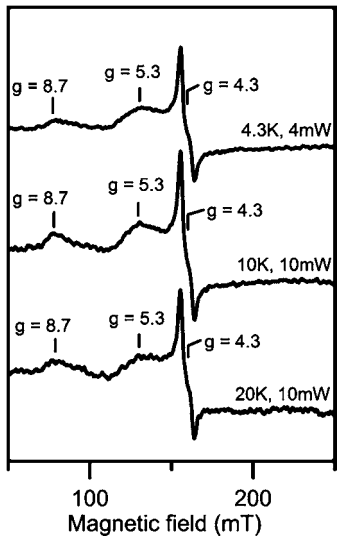

Figure 3. X-band EPR evidence for a $S = 5/2$ linear $[Fe_3S_4]^+$ cluster in *Sc* Grx5. The conditions were microwave frequency, 9.60 GHz; modulation frequency, 100 kHz; modulation amplitude, 0.65 mT.

$D > 0$ cm^{-1}, which predicts *g*-values at 4.42, 4.27, and 4.15 for the middle doublet of the ground-state manifold and a weak low-field absorption shaped component at $g \sim 9.6$ arising from the lowest doublet. The broad absorption-shaped low-field features centered at $g = 8.7$ and 5.3 are interpreted in terms of substantial *D*-strain,[33] i.e., distributed *D* and *E* values resulting from inhomogeneity in the linear $[Fe_3S_4]^+$ clusters in frozen solution. Similar *D*-strain effects on the observed EPR spectrum have been reported for the linear $[Fe_3S_4]^+$ clusters in synthetic complexes and in alkaline aconitase.[31,34]

VTMCD spectroscopy provides a selective probe of the electronic transitions and ground-state properties of paramagnetic chromophores as well as a useful method for assessing cluster type for paramagnetic Fe−S clusters. Mössbauer studies have shown ∼70% of the Fe is in the form of paramagnetic linear $[Fe_3S_4]^+$ clusters with the remaining Fe in the form of $S = 0$ $[Fe_2S_2]^{2+}$ and $[Fe_4S_4]^{2+}$ clusters and a high-spin $S = 2$ Fe^{2+} species. However, since the former two types of clusters are diamagnetic, and the Fe^{2+} species would not be expected to exhibit significant VTMCD intensity in the visible region, their presence does not interfere with low-temperature MCD characterization of the paramagnetic linear $[Fe_3S_4]^+$ cluster in *Sc* Grx5 in the visible region. VTMCD spectra recorded at 6 T for temperatures in the range 1.7 to 50 K consist of three consecutive negative features between 300 and 400 nm, three consecutive pronounced positive bands in the region between 400 and 550 nm, and multiple less intense features with alternative negative and positive signs with decreasing energy (Figure 4). These temperature-dependent MCD bands facilitate resolution of the overlapping S-to-Fe(III) charge-transfer transitions that comprise the UV−vis absorption spectrum. More importantly, the pattern and intensity of the low-temperature MCD spectra of the linear $[Fe_3S_4]^+$ cluster in *Sc* Grx5 are strikingly similar to those previously reported for synthetic and protein-bound linear $[Fe_3S_4]^+$ clusters[34] and are distinct from other structurally well-defined biological Fe−S clusters.

Information on the ground-state electronic properties of the linear $[Fe_3S_4]^+$ cluster in *Sc* Grx5 was provided by the VTVH MCD magnetization studies. In accord with an $S = 5/2$ ground-

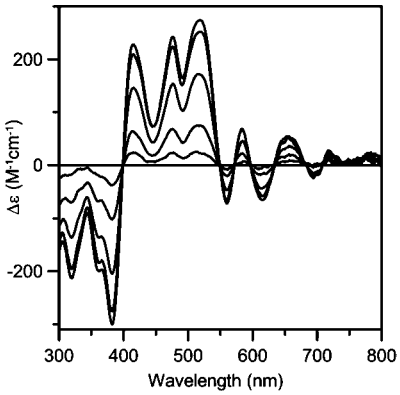

Figure 4. VTMCD spectra of the linear $[Fe_3S_4]^+$ cluster in *Sc* Grx5. The sample was in 100 mM Tris-HCl buffer with 1 mM GSH at pH 7.8, with 50% v/v ethylene glycol. Spectra were recorded for sample in 1 mm cuvette at 1.70, 4.22, 10.0, 25.0, and 50.0 K in a magnetic field of 6 T. All MCD bands increase in intensity with decreasing temperature.

state spin, the VTVH MCD saturation magnetization data collected at 415 nm consist of a nested set of field-dependent plots at fixed temperatures, that results from differential Boltzmann population and field-induced mixing of zero-field components, see Figure 5.[35] The VTVH MCD saturation

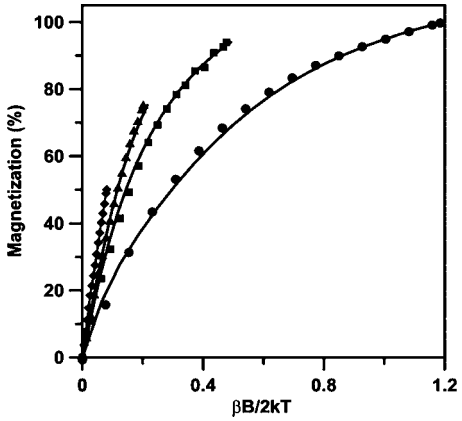

Figure 5. VHVT MCD saturation magnetization data for the linear $[Fe_3S_4]^+$ center in *S. cerevisiae* Grx5. Sample is as described in Figure 4. MCD intensity at 415 nm was monitored as a function of magnetic field, from 0 to 6 T, at temperatures of 1.70 K (●), 4.22 K (■), 10.0 K (▲) and 25.0 K (◆). Solid lines are theoretical fits for a rhombic S = 5/2 ground state with zero-field splitting parameters D = +0.6 cm^{-1} and E/D = 0.31, an isotropic real g-value of 2.0023, and a predominantly y-polarized electronic transition (36% M_{xy}; 6% M_{xz}; 58% M_{yz}). The fitting procedure used was that developed by Neese and Solomon.[22]

magnetization data collected at 415 nm were fit to a rhombic S = 5/2 ground state (E/D = 0.31) by varying the transition polarizations and magnitude of the axial zero-field splitting parameter, D. The best fit, shown in Figure 5, was obtained for a predominantly y-polarized electronic transition (36% M_{xy}; 6% M_{xz}; 58% M_{yz}) with D = 0.6 cm^{-1}. The Mössbauer spectra of the linear $[Fe_3S_4]^+$ cluster in *Sc* Grx5 were analyzed using a value of 2.0 cm^{-1} for the axial zero-field splitting parameter D. However, VTVH MCD saturation magnetization data are quite sensitive to the values of D, with satisfactory fits only possible with D = 0.6 ± 0.2 cm^{-1}, whereas the Mössbauer spectra were quite insensitive to the value of D. This value of D is similar to those determined using VTVH MCD saturation magnetization for the aconitase linear $[Fe_3S_4]^+$ cluster, D = 1.5 ± 0.2 cm^{-1}, and the synthetic analog complex, D = 0.7 ± 0.2 cm^{-1}.[34]

To our knowledge, the vibrational properties of linear-type $[Fe_3S_4]^+$ centers have not been previously investigated. As the UV−vis absorption, EPR, VTMCD, and Mössbauer results presented above provide compelling evidence for a linear $[Fe_3S_4]^+$ cluster as the predominant type of Fe−S cluster in *Sc* Grx5, the Fe−S stretching modes of the linear $[Fe_3S_4]^+$ cluster were assessed by resonance Raman spectroscopy using visible excitation into S-to-Fe(III) charge transfer bands. Resonance Raman spectra of the linear $[Fe_3S_4]^+$ cluster-bound *Sc* Grx5 in the Fe−S stretching region, using 406.7, 457.9, 487.9, and 514.5-nm excitation, are shown in Figure 6. To facilitate

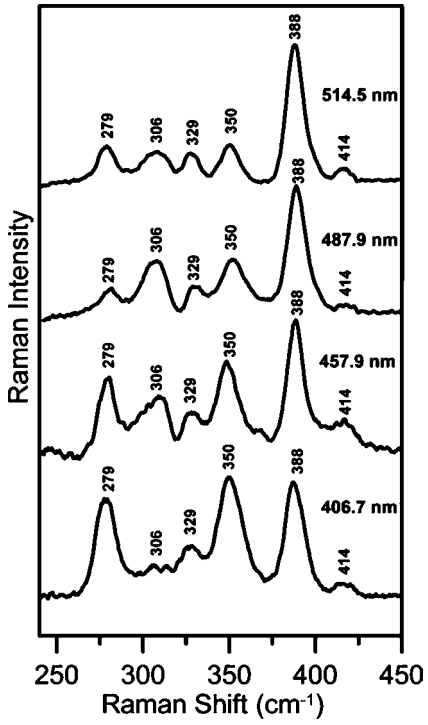

Figure 6. Resonance Raman spectra of linear $[Fe_3S_4]^+$ cluster-bound *Sc* Grx5 with 406.7, 457.9, 487.9, and 514.5 nm laser excitations. The sample contained ~2 mM of linear $[Fe_3S_4]^+$ cluster in 100 mM Tris-HCl buffer with 1 mM GSH at pH 7.8 and was in the form of a frozen droplet at 17 K. Each spectrum is the sum of 100 individual scans with each scan involving photon counting for 1 s at 0.5 cm^{-1} increment with 7 cm^{-1} spectral resolution. Bands due to ice lattice modes have been subtracted from all spectra.

assignment of normal modes primarily involving Fe−S^b and Fe−S^t stretching, resonance Raman spectra of samples reconstituted with natural abundance (~95% ^{32}S, ~4% ^{34}S) and isotopically enriched (>95%) ^{34}S bridging sulfides are compared in Figure 7. Significantly, the resonance Raman enhancement profiles, frequencies, and pattern of $^{32/34}S$ isomer shifts are quite distinct compared to those of other types of biological Fe−S clusters, including $[Fe_2S_2]^{2+}$, $[Fe_4S_4]^{2+}$, and cubane-type $[Fe_3S_4]^+$ clusters. Under idealized D_{2d} symmetry the $Fe_3S^b{}_4S^t{}_4$ cluster is expected to have 6 predominantly Fe−S^b stretching modes ($2A_1$, $2B_2$, 2E) and three predominantly Fe−S^t stretching modes (A_1, B_2, E). Definitive band assignments based on normal mode calculations have not been carried out thus far, because of possible contributions from the minority

dx.doi.org/10.1021/ja407059n | J. Am. Chem. Soc. 2013, 135, 15153−15164

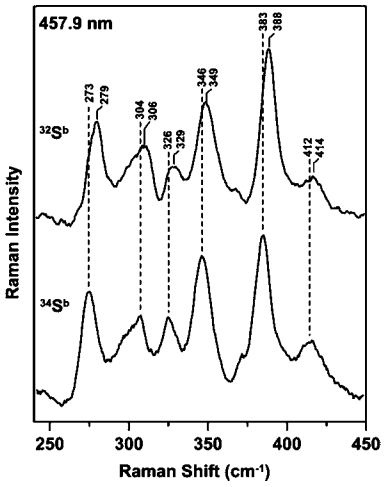

Figure 7. Resonance Raman spectra of the $^{32}S^b$- and $^{34}S^b$-reconstituted linear $[Fe_3S_4]^+$ cluster in *Sc* Grx5 showing $^{34}S/^{32}S$ isotopic shifts. Spectra were obtained with 457.9 nm laser excitation. The conditions were the same as in Figure 6.

$[Fe_2S_2]^{2+}$ and $[Fe_4S_4]^{2+}$ clusters that are present in the samples. Nevertheless, based on the large magnitude of the $^{34/32}S$ isotope shifts (~5 cm^{-1}), the intense band at 388 cm^{-1} is primarily attributed to the A_1 symmetric breathing mode of the $Fe(\mu\text{-}S^b)_2Fe(\mu\text{-}S^b)_2Fe$ core with the *S* motions along the *x* and *y* directions (i.e., perpendicular to the Fe−Fe−Fe axis), and the band at 279 cm^{-1} is primarily attributed to the A_1 symmetric breathing mode of the $Fe(\mu\text{-}S^b)_2Fe(\mu\text{-}S^b)_2Fe$ core with the *S* motions along the *z* direction (i.e., parallel to the Fe−Fe−Fe axis). The latter is downshifted ~100 cm^{-1}, since it requires significant movement of the outer Fe atoms. The former occurs at a similar frequency to that of the symmetric breathing mode of the $Fe(\mu\text{-}S^b)_2Fe$ core in biological and synthetic $[Fe_2S_2]^{2+}$ clusters (A_{1g} under idealized D_{2h} symmetry) which occur in the range 387−401 cm^{-1}.[36−38]

In Vitro Assembly of a $[Fe_4S_4]^{2+}$ Cluster on Sc Grx5. To further explore the types and properties of Fe−S clusters assembled in *Sc* Grx5, *in vitro* cysteine desulfurase-mediated cluster reconstitution was carried out under anaerobic conditions with 5 mM DTT in place of GSH and in the absence of DTT or GSH, using samples pretreated with TCEP. In both cases, reconstitution resulted in the formation of an identical Fe−S center that is different from the linear $[Fe_3S_4]^+$ cluster as evidenced by the combination of UV−vis absorption, Mössbauer, and resonance Raman spectroscopic studies. The absorption spectrum of the Fe−S cluster assembled in the absence of GSH (red trace in Figure 1) exhibits a broad band in the visible region centered at 400 nm (A_{400}/A_{280} = 0.43) that is characteristic of a $[Fe_4S_4]^{2+}$ cluster.[39] Protein and Fe analyses indicated 2.5 ± 0.3 Fe per *Sc* Grx5 monomer, suggesting ~1 $[Fe_4S_4]^{2+}$ cluster per *Sc* Grx5 homodimer. Moreover, the extinction coefficient at 400 nm, 16.9 $mM^{-1}cm^{-1}$, based on the *Sc* Grx5 dimer concentration, is indicative of ~1 $[Fe_4S_4]^{2+}$ cluster per *Sc* Grx5 dimer.[26,39,40] The CD spectrum of the $[Fe_4S_4]^{2+}$ cluster in the UV−vis region is very weak and featureless, which is also characteristic of many biological $[Fe_4S_4]^{2+}$ clusters.[41]

Mössbauer analysis of ^{57}Fe-reconstituted *Sc* Grx5 in the absence of GSH provided more definite confirmation of the presence of a $[Fe_4S_4]^{2+}$ cluster in *Sc* Grx5. The 4.2 K Mössbauer spectrum recorded with a parallel applied field of 50 mT is best simulated as the sum of two equal intensity quadrupole doublets with the following parameters: ΔE_Q = 1.05 mm/s, δ = 0.41 mm/s, Γ = 0.45 mm/s for doublet 1 and ΔE_Q = 1.16 mm/s, δ = 0.49 mm/s, Γ = 0.36 mm/s for doublet 2 (Figure 8). The parameters are consistent with an all-

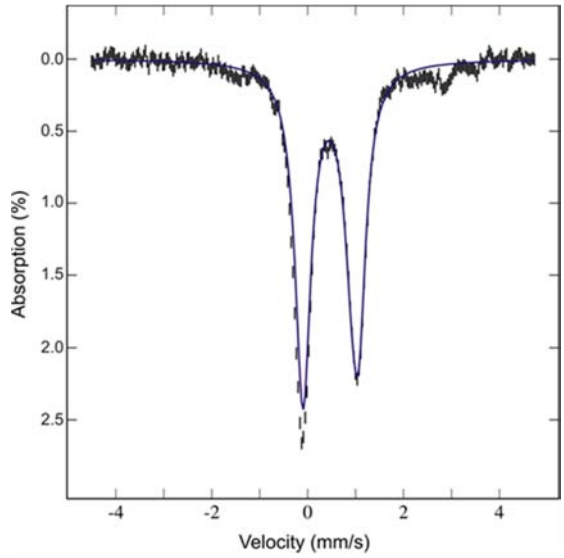

Figure 8. Mössbauer spectrum of $[Fe_4S_4]^{2+}$ cluster-bound *Sc* Grx5. The spectrum was recorded at 4.2 K with an applied field of 50 mT parallel to the γ-radiation. The solid blue line is a theoretical simulation of 92% of the Fe in the form of $[Fe_4S_4]^{2+}$ clusters composed of two overlapping quadrupole doublets with the following parameters: ΔE_Q = 1.05 mm/s, δ = 0.41 mm/s, Γ= 0.45 mm/s for doublet 1 and ΔE_Q = 1.16 mm/s, δ = 0.49 mm/s, Γ = 0.36 mm/s for doublet 2.

cysteinyl ligated $[Fe_4S_4]^{2+}$ cluster with an S = 0 ground state resulting from antiferromagnetic interaction between two valence delocalized $[Fe_2S_2]^+$ fragments.[42,43] Analysis of the Mössbauer spectrum revealed that 92% of the total ^{57}Fe absorption in the sample is present in the form of $[Fe_4S_4]^{2+}$ clusters, while the remaining 8% can be attributed to adventitiously bound Fe^{2+} species. The presence of other Fe-containing species was not detected.

The vibrational properties of the $[Fe_4S_4]^{2+}$ cluster in *Sc* Grx5 were also investigated by low-temperature resonance Raman spectroscopy. Cubane-type $[Fe_4S_4]^{2+}$ clusters generally exhibit lower resonance enhancement compared to other types of biological Fe−S clusters in the Fe−S stretching region (240−450 cm^{-1}), and the resonance Raman spectrum of the $[Fe_4S_4]^{2+}$ center in *Sc* Grx5 using 457.8 and 487.9 nm excitation has exceptionally weak resonance enhancement. Nevertheless, the spectrum shown in Figure 9 is characteristic of a $[Fe_4S_4]^{2+}$ cluster and can be reasonably assigned by comparison to $[Fe_4S_4]$-ferredoxins and appropriate analog complexes.[44] Based on extensive spectroscopic studies on biological and synthetic $[Fe_4S_4]$ clusters, the frequency of the totally symmetric Fe and bridging S breathing mode can be used to indicate cluster ligation, 333−339 cm^{-1} for a $[Fe_4S_4]$ cluster with complete cysteinyl ligation, and 340−343 cm^{-1} for a $[Fe_4S_4]$ cluster with a unique Fe site with OH^-, serinate, or aspartate ligation.[45,46] Thus the frequency of the totally symmetric breathing mode at 338 cm^{-1} observed for the $[Fe_4S_4]^{2+}$ cluster in *Sc* Grx5 suggests complete cysteinyl ligation for the $[Fe_4S_4]^{2+}$ cluster. The Raman band at 352 cm^{-1} is assigned to an asymmetric Fe−S(Cys) stretching mode, however the intensity of this band in

dx.doi.org/10.1021/ja407059n | J. Am. Chem. Soc. 2013, 135, 15153−15164

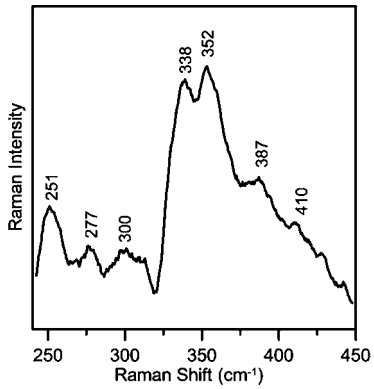

Figure 9. Resonance Raman spectrum of $[Fe_4S_4]^{2+}$ cluster-bound *Sc* Grx5 with 487.9 nm laser excitation. The sample contained ~2 mM of $[Fe_4S_4]^{2+}$ cluster in 100 mM Tris-HCl buffer with 1 mM DTT at pH 7.8 and was in the form of a frozen droplet at 17 K. The spectrum is the sum of 100 individual scans with each scan involving photon counting for 1 s at 0.5 cm^{-1} increment with 7 cm^{-1} spectral resolution. Bands due to ice lattice modes have been subtracted.

$[Fe_4S_4]$-Grx5 is anomalously high compared to that of other biological $[Fe_4S_4]^{2+}$ clusters.[44] Both the weak resonance enhancement and anomalous intensity of the asymmetric Fe−S(Cys) stretching mode are tentatively attributed to changes in cluster distortion or environment resulting from a subunit-bridging $[Fe_4S_4]^{2+}$ cluster.

Activation of Apo-Aconitase Using $[Fe_4S_4]^{2+}$ Cluster-Bound Sc Grx5. To investigate the possibility that the $[Fe_4S_4]^{2+}$ cluster-bound form of *Sc* Grx5 is competent for *in vitro* activation of apo-aconitase, 4 μM apo-aconitase was incubated with 3-fold excess of $[Fe_4S_4]$-Grx5 (12 μM in $[Fe_4S_4]^{2+}$ clusters), and aconitase enzymatic activity was assessed periodically over a 90-min time period. Figure 10 shows the time-dependent apo-aconitase activation when it is mixed with $[Fe_4S_4]$-Grx5. Analysis based on second-order kinetics and the initial concentrations of $[Fe_4S_4]^{2+}$ clusters in *Sc* Grx5 and apo-aconitase indicates a second-order rate constant of 6.0 × 10^3 $M^{-1}min^{-1}$ at room temperature, which implies activation by intact cluster transfer, since it is at least an order of magnitude greater than the rate of aconitase activation with equivalent amounts of Fe^{2+} and S^{2-} ions. Intact cluster transfer is also indicated by the observation that the rate of aconitase activation was not significantly perturbed by the presence of 1 mM EDTA in the reaction mixture. The rate constant for $[Fe_4S_4]$-Grx5 aconitase activation is comparable to that observed under analogous conditions using a $[Fe_4S_4]^{2+}$ cluster-loaded form of *A. vinelandii* IscU, 1.1 × 10^4 $M^{-1}min^{-1}$, but is an order of magnitude slower than that reported using $[Fe_4S_4]$-NfuA from *A. vinelandii* as the cluster donor, 6.0 × 10^4 $M^{-1}min^{-1}$.[24,26] The slower rate of cluster transfer may reflect using $[Fe_4S_4]$ cluster-containing *Sc* Grx5 as the donor for apo *A. vinelandii* aconitase. However, these results indicate that the $[Fe_4S_4]^{2+}$ cluster-bound form of *Sc* Grx5 is competent for activation of apo-aconitase *in vitro* via intact $[Fe_4S_4]$ cluster transfer.

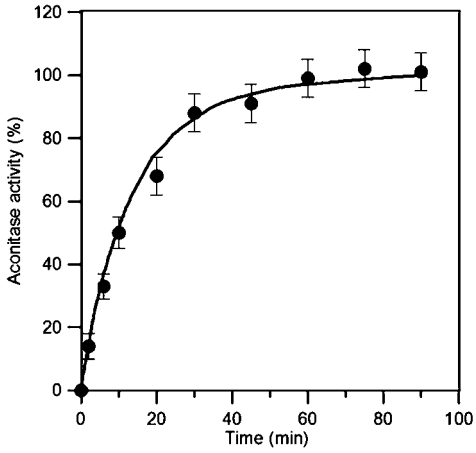

Figure 10. Activation of apo-aconitase using $[Fe_4S_4]^{2+}$ cluster-bound *Sc* Grx5. Apo-aconitase (4 μM) was incubated with $[Fe_4S_4]^{2+}$ cluster-bound *Sc* Grx5 (12 μM in $[Fe_4S_4]^{2+}$ cluster concentration) at room temperature under anaerobic conditions. Aliquots were withdrawn after 2, 6, 10, 30, 45, 60, 75, and 90 min, and aconitase activity was immediately measured. The solid line is best fit to second-order kinetics with rate constant of 6.0 × 10^3 M^{-1} min^{-1}.

Investigation of Cluster Ligation in Sc Grx5. As the spectroscopic properties reported herein indicate that both the linear $[Fe_3S_4]^+$ and $[Fe_4S_4]^{2+}$ clusters assembled in *Sc* Grx5 are best interpreted in terms of complete cysteinyl-ligation, site-directed mutagenesis studies were undertaken to address the specific cysteines involved in cluster ligation. *Sc* Grx5 without the mitochondrial targeting sequence possesses two cysteine residues at positions 33 and 90 (recombinant *S. cerevisiae* Grx5 numbering). The active-site cysteine (Cys33) is conserved in all monothiol CGFS-Grxs and is involved in ligating $[Fe_2S_2]^{2+}$ clusters, whereas Cys90 is partially conserved in CGFS-type Grxs.[14,47] In order to address the cluster ligation in *Sc* Grx5, a C90S mutant was generated to investigate the ability of this variant to incorporate Fe−S clusters. Following *in vitro* cysteine desulfurase-mediated Fe−S cluster reconstitution in the presence of 3 mM GSH, the *Sc* Grx5 C90S variant was found to incorporate a linear $[Fe_3S_4]^+$ cluster, as evidenced by the identical UV−vis absorption characteristics compared to that of the linear $[Fe_3S_4]^+$ cluster center in the wild type *Sc* Grx5 (Figure S3). However, the C90S mutant failed to assemble a $[Fe_4S_4]^{2+}$ cluster during cysteine desulfurase-mediated Fe−S cluster reconstitution in the presence of 5 mM DTT, as evidenced by the lack of any visible absorption bands after removal of the excess reagents in the reconstitution mixture by anaerobic gel filtration. Thus the site-directed mutagenesis studies suggest that the partially conserved cysteine is required for the incorporation of the $[Fe_4S_4]^{2+}$ cluster in *Sc* Grx5, but not the linear $[Fe_3S_4]^+$ cluster. Coupled with the analytical data that indicate approximately one $[Fe_4S_4]^{2+}$ cluster per *Sc* Grx5 homodimer, the data suggest that the ligation of the $[Fe_4S_4]^{2+}$ cluster in *Sc* Grx5 involves both the active-site cysteine and the partially conserved cysteine of two *Sc* Grx5 monomers.

Based on the ability of the C90S mutant to accommodate a linear $[Fe_3S_4]^+$ cluster, the requirement of GSH for cluster formation, and the stoichiometry of one cluster per dimer, it seemed likely that the linear $[Fe_3S_4]^+$ cluster in *Sc* Grx5 is coordinated by the active-site cysteine of two CGFS-Grx monomers and two external GSH molecules, similar to the ligation of the $[Fe_2S_2]^{2+}$ cluster in other CGFS Grxs.[2,15] Moreover, the presence of two GSH molecules per linear $[Fe_3S_4]^+$ cluster in *Sc* Grx5 was confirmed by GSH analysis of the as purified apo protein and a reconstituted sample that was ~80% cluster-loaded based on UV−vis absorption data (A_{403}/A_{280} = 0.40). Apo *Sc* Grx5 was found to contain 1.0 ± 0.2 GSH/monomer, in accord with the mass spectrometry analysis

dx.doi.org/10.1021/ja407059n | J. Am. Chem. Soc. 2013, 135, 15153−15164

(see Figure S1). After correcting for the presence of two GSH/$[Fe_2S_2]^{2+}$ cluster and one GSH/apo monomer and assessing the $[Fe_3S_4]^{+}$ cluster concentration in the sample based on the total Fe content and the cluster composition determined by Mössbauer spectroscopy (vide supra), the GSH analysis indicated 2.0 ± 0.3 GSH/$[Fe_3S_4]^{+}$ cluster.

DISCUSSION

The widely accepted and evolutionarily conserved role for CGFS-Grxs in facilitating the trafficking of Fe−S clusters preassembled on IscU-type scaffold proteins was initially revealed using *S. cerevisiae* mitochondrial Grx5 as a model protein.[5,6,10] While the majority of other CGFS-Grxs investigated thus far have demonstrated the ability to incorporate a $[Fe_2S_2]^{2+}$ cluster at the homodimer interface, based on spectroscopic characterization[7,8,16,28,48] and crystal structures for *E. coli* Grx4 and human Glrx5,[2,15] the nature of the cluster(s) assembled on *S. cerevisiae* mitochondrial Grx5 had not been adequately addressed prior to this work. Using the combination of UV−vis absorption/CD/VTMCD, EPR, Mössbauer and resonance Raman spectroscopies, we have demonstrated that recombinant *S. cerevisiae* mitochondrial Grx5 is a versatile Fe−S protein able to accommodate linear $[Fe_3S_4]^{+}$, cubane-type $[Fe_4S_4]^{2+}$, and $[Fe_2S_2]^{2+}$ clusters. This is the first report that monothiol Grxs can bind linear $[Fe_3S_4]^{+}$ and cubane-type $[Fe_4S_4]^{2+}$ clusters. Moreover, the results indicate that the Fe−S cluster content, previously reported for many CGFS-Grxs either as purified or reconstituted in the presence of GSH, has been misinterpreted in terms of $[Fe_2S_2]^{2+}$ clusters rather than linear $[Fe_3S_4]^{+}$ clusters or mixtures of linear $[Fe_3S_4]^{+}$ and $[Fe_2S_2]^{2+}$ clusters.

In two separate studies, Picciocchi et al.[16] and Uzarska et al.[10] have reported purification of an Fe−S cluster-bound form of recombinant *Sc* Grx5. In the study reported by Picciocchi et al., the type of the cluster was interpreted as a $[Fe_2S_2]$ cluster solely on the basis of the UV−vis absorption spectrum comprising primarily a well-resolved band at ∼410 nm[16] that could equally be attributed, at least in part, to the Soret band of minor heme impurity. In contrast, the UV−vis absorption spectrum reported by Uzarska et al. for the as-isolated cluster-bound form of *Sc* Grx5 was attributed to a $[Fe_2S_2]^{2+}$ center[10] but is predominantly or exclusively a linear-type $[Fe_3S_4]^{+}$ center, based on the work reported herein. In neither case were the extent of cluster loading assessed based on protein, iron, and sulfide determinations. Furthermore, despite extensive efforts involving varying pH, GSH concentrations, and temperature, we have failed to obtain *Sc* Grx5 containing predominantly $[Fe_2S_2]^{2+}$ clusters using our established *in vitro* cluster reconstitution protocols for incorporating $[Fe_2S_2]^{2+}$ clusters in CGFS-Grxs.[7,28]

Linear-type $[Fe_3S_4]^{+}$ clusters were initially characterized as synthetic complexes,[30] and the first protein-bound linear $[Fe_3S_4]^{+}$ cluster was later discovered in partially unfolded beef heart aconitase via incubation under alkaline conditions (pH > 9.5) or treating with high concentrations of urea (4−8 M).[31] The only other well-documented examples of protein-bound linear $[Fe_3S_4]^{+}$ clusters prior to this study were reconstituted human cytosolic iron-responsive protein 1 (IRP1) at pH 7.5,[49] and as one of the many types of clusters in the as-isolated form of the pyruvate formate lyase activating enzyme (PFL-AE).[50] We have demonstrated in this work that *Sc* Grx5 containing a linear $[Fe_3S_4]^{+}$ cluster as the dominant Fe-containing species is observed when the apo protein is reconstituted under anaerobic conditions and in aerobically purified samples after prolonged exposure of the cell-free extract to air, both in the presence of GSH. Cysteine mutagenesis studies, coupled with Fe, protein, and GSH determinations, suggest that the linear $[3Fe\text{-}4S]^{+}$ cluster is ligated at the subunit interface of a homodimer by the two cysteines of the CGFS active-site motif and two GSHs. The excited- and ground-state electronic properties of the linear $[Fe_3S_4]^{+}$ cluster in *Sc* Grx5 have been characterized in detail using UV−vis absorption, CD and VTMCD, EPR, and Mössbauer spectroscopies. The results are strikingly similar to those obtained for structurally characterized synthetic linear $[Fe_3S_4]^{+}$ clusters and protein-bound linear $[Fe_3S_4]^{+}$ clusters with complete thiolate ligation and indicate a $S = 5/2$ linear $[Fe_3S_4]^{+}$ cluster in a rhombic ($E/D = 0.31$) environment.[30−32,34] Our results taken together with those of Uzarska et al.[10] indicate that recombinant *Sc* Grx5 has much greater affinity for binding linear $[Fe_3S_4]^{+}$ clusters than $[Fe_2S_2]^{2+}$ clusters both as purified and under reconstitution conditions.

The ability to incorporate linear $[Fe_3S_4]^{+}$ clusters in CGFS-Grxs is not unique to *S. cerevisiae* Grx5. Based on the distinctive UV−vis absorption and/or Mössbauer properties of linear $[Fe_3S_4]^{+}$ clusters characterized in this work, it is now evident many of the recombinant CGFS-Grx clusters that have been assigned exclusively as $[Fe_2S_2]^{2+}$ clusters in the literature actually contain linear $[Fe_3S_4]^{+}$ clusters or mixtures of $[Fe_2S_2]^{2+}$ and linear $[Fe_3S_4]^{+}$ clusters in either their aerobically isolated or anaerobic reconstituted forms. These include *Synechocystis* Grx3, *A. thaliana* GrxS14 (annotated as *At* Grx5p), *Gloeobacter violaceus* Grx3,[16] human Glrx5,[51] human Glrx3,[52] and *E. coli* Grx4.[48] Moreover, recent work from our laboratory has established conditions for preparing *A. thaliana* GrxS14 and GrxS16 and *A. vinelandii* Grx5 in forms containing exclusively $[Fe_2S_2]^{2+}$ clusters or variable mixtures of $[Fe_2S_2]^{2+}$ and linear $[Fe_3S_4]^{+}$ clusters.[53,54] Hence, we conclude that the ability to incorporate a linear $[Fe_3S_4]^{+}$ cluster is likely to be a common attribute of many, if not all, CGFS-Grxs.

To our knowledge, linear-type $[Fe_3S_4]^{+}$ clusters are not associated with any physiological function. Thus the significance of the presence of linear $[Fe_3S_4]^{+}$ clusters in CGFS-Grxs remains to be established. However, it may be related to the inherent stability of linear $[Fe_3S_4]^{+}$ clusters under aerobic conditions and their established ability to undergo cluster conversions to yield $[Fe_2S_2]^{2+}$ clusters by loss of Fe^{3+} and S^{2-} or $[Fe_4S_4]^{2+}$ clusters by reductive addition of Fe^{2+}, as revealed first by studies of synthetic clusters[30] and subsequently in aconitase.[31] Our observation that linear $[Fe_3S_4]^{+}$ clusters are formed in heterologously expressed *Sc* Grx5 during exposure of the cell free extract to air, suggest that linear $[Fe_3S_4]^{+}$ clusters formed during oxidative unfolding and degradation of Fe−S proteins under oxidative stress conditions. This is also supported by the formation of linear $[Fe_3S_4]^{+}$ clusters or protein associated linear polymers based on linear $[Fe_3S_4]^{+}$ cluster units, during unfolding of ferredoxins under oxidative conditions.[55−58] Moreover, our recent studies of *Av* Grx5 and Grx-nif, the two CGFS-Grxs in *A.vinelandii*,[54] coupled with the UV−vis spectra of CGFS-Grxs reported by Picciocchi et al.,[16] indicate that linear $[Fe_3S_4]^{+}$ clusters are only observed in recombinant CGFS-Grxs purified under aerobic conditions. Hence we conclude that the ability to accommodate linear $[Fe_3S_4]^{+}$ clusters in the presence of GSH implies a role for CGFS-Grxs in scavenging and recycling Fe−S clusters released during protein unfolding under oxidative conditions to avoid

potential toxicity caused by Fe accumulation in the cell. This is also consistent with the phenotype of mitochondrial iron overload and increased sensitivity to oxidative stress that is associated with *Sc* Grx5 deficiency.[5]

Reconstitution of *Sc* Grx5 in the absence of GSH yielded a homogeneous form containing one all-cysteinate-ligated $S = 0$ $[Fe_4S_4]^{2+}$ cluster per homodimer, as evidenced by protein and Fe analyses as well as UV−vis absorption, Mössbauer, and resonance Raman spectroscopic results. In addition, mutational studies indicate that the semiconserved Cys90 is essential for $[Fe_4S_4]^{2+}$ cluster assembly. Taken together, the spectroscopic, mutagenesis, and analytical data suggest that the $[Fe_4S_4]^{2+}$ cluster is ligated at the subunit interface of a homodimer by the CGFS active-site cysteine, Cys33, and semiconserved cysteine, Cys90. The close spatial proximity of these two cysteines in the oxidized the apo form of *Sc* Grx5 was previously demonstrated by biochemical characterization which revealed that Cys90 is capable of forming an intraprotein disulfide with the active-site cysteine residue, Cys33.[1]

In accord with the *in vivo* studies *S. cerevisiae* that demonstrated the requirement of Grx5 in maintaining mitochondrial aconitase enzymatic activity,[5] we have shown in this work that the $[Fe_4S_4]^{2+}$ cluster-bound form of *Sc* Grx5 is competent for restoring the activity of apo *Av* aconitase protein *in vitro* via intact cluster transfer. This observation, coupled with the intrinsic cysteinyl-ligation scheme for the $[Fe_4S_4]^{2+}$ cluster in *Sc* Grx5, raises the possibility of CGFS-Grxs participating in the maturation of $[Fe_4S_4]^{2+}$ cluster-containing proteins in mitochondria in a GSH-independent fashion, possibly as a carrier protein to mediate the transfer of preassembled $[Fe_4S_4]^{2+}$ clusters to target proteins. This hypothesis is also in agreement with the discovery that GSH is not required for the maturation of mitochondrial Fe−S proteins,[59] and the observation that *Sc* Grx5 is involved in the maturation of both $[Fe_2S_2]$ and $[Fe_4S_4]$ proteins in *S. cerevisiae*.[10] However, mutation of Cys90 which is required for $[Fe_4S_4]$ cluster assembly, does not induce the phenotypic effects induced by *grx5* deletion in *S. cerevisiae*,[14] which appears to argue against a physiological role for the $[Fe_4S_4]^{2+}$ cluster-bound form of Grx5 in yeast mitochondria. Clearly more work is required with a wider range of CGFS-Grxs to establish the physiological relevance of $[Fe_4S_4]^{2+}$ cluster-bound forms.

The majority of CGFS-Grxs characterized thus far were found to accommodate a subunit-bridged $[Fe_2S_2]^{2+}$ cluster ligated by the active-site cysteine of two Grx monomers and two GSH molecules. However, we have yet to obtain a homogeneous $[Fe_2S_2]^{2+}$ cluster-containing form of recombinant *Sc* Grx5. Mössbauer studies of recombinant *Sc* Grx5 reconstituted in the presence of GSH revealed a minor contribution (11% of the total ^{57}Fe absorption) of a quadrupole doublet corresponding to a protein-bound $[Fe_2S_2]^{2+}$ cluster. However, based on the recent dramatic enhancement of *in vitro* $[Fe_2S_2]^{2+}$ cluster transfer from *Av* IscU to *Av* Grx5 in the presence of the dedicated *Av* cochaperones HscA/HscB and ATP,[8] it is clearly possible that the low levels of cluster-bound *Sc* Grx5 that are observed *in vivo* based on ^{55}Fe immunoprecipitation studies, involve $[Fe_2S_2]$ clusters that are specifically transferred from Isu1 in an ATP-dependent process in which *Sc* Grx5 is directly associated with Ssq1, the yeast homologue of HscA.[10] Hence the inability to express the $[Fe_2S_2]^{2+}$ cluster-containing form of *Sc* Grx5 in *E. coli*, may reflect the inability of *E. coli* HscA to substitute for *Sc* Ssq1 in facilitating ATP-dependent $[Fe_2S_2]^{2+}$ cluster transfer from *E. coli* IscU to *Sc* Grx5. Support for the specificity of *Sc* Ssq1, as compared to the bacterial HscA, in promoting $[Fe_2S_2]^{2+}$ cluster transfer from *Sc* Isu1 to *Sc* Grx5 comes for the observation that *Av* HscA/HscB/ATP did not facilitate $[Fe_2S_2]^{2+}$ cluster transfer from *Av* IscU to *Sc* Grx5 using the same conditions that were so effective for promoting rapid and quantitative transfer to *Av* Grx5.[8] UV−vis CD studies indicate that the $[Fe_2S_2]^{2+}$ clusters originally on *Av* IscU gradually degrade over a 3 h time period, but that the product of the reaction was *Sc* Grx5 with low occupancy of a linear $[Fe_3S_4]^{+}$ cluster based on comparison with the CD spectra shown in Figure 1, see Figure S4. We conclude that *Sc* Grx5 has a greater affinity for linear $[Fe_3S_4]^{+}$ than $[Fe_2S_2]^{2+}$ clusters compared to most other GCFS-Grxs, but that the ability of *Sc* Grx5 to bind and transfer $[Fe_2S_2]^{2+}$ clusters assembled on *Sc* Isu1 cannot be ruled out. The conditions for obtaining a homogeneous $[Fe_2S_2]^{2+}$ cluster-containing *Sc* Grx5 will require further investigation, including *in vitro* cluster transfer from *Sc* $[Fe_2S_2]$-Isu1 in the presence of *Sc* Ssq1/Jaq1/ATP.

CGFS-Grxs are clearly attracting increasing attention due to their involvement in Fe−S cluster biogenesis in prokaryotes and eukaryotes and the regulation of Fe-trafficking in eukaryotes.[7,8,10,47,60,61] Moreover, the most recent *in vivo* study has demonstrated that *Sc* Grx5 is required for the maturation of both mitochondrial and cytosolic $[Fe_2S_2]$ and $[Fe_4S_4]$ cluster-requiring proteins.[10] The investigation of the Fe−S cluster-bound forms of recombinant *Sc* Grx5 reported in this work has revealed the ability of CGFS-Grxs to accommodate three different types of Fe−S clusters, i.e., linear $[Fe_3S_4]^{+}$, $[Fe_4S_4]^{2+}$, and $[Fe_2S_2]^{2+}$ clusters. Thus there is clearly a pressing need to identify the physiologically relevant Fe−S cluster-bound forms of CGFS-Grxs and to investigate the Fe−S cluster structure−function relationships of CGFS-Grxs in specific organisms and organelles.

■ ASSOCIATED CONTENT

Supporting Information

Table of primers used for *Sc* Grx5 cloning and mutagenesis, mass spectrum of apo *Sc* Grx5, UV−vis CD for the formation of linear $[Fe_3S_4]^{+}$ clusters on *Sc* Grx5 in cell-free extracts exposed to air, UV−vis absorption evidence for the formation of linear $[Fe_3S_4]^{+}$ clusters on *Sc* Grx5 C90S mutant, and UV−vis CD time course of attempted cluster transfer from *A. vinelandii* $[Fe_2S_2]$-IscU to apo *Sc* Grx5 in the presence of HscA/HscB/MgATP and GSH. This material is available free of charge via the Internet at http://pubs.acs.org.

■ AUTHOR INFORMATION

Corresponding Author

mkj@uga.edu

Author Contributions

[‖]These authors contributed equally.

Notes

The authors declare no competing financial interest.

■ ACKNOWLEDGMENTS

This work was supported by grants from the National Institutes of Health (GM62524 to M.K.J. and GM47295 to B.H.H.) and the Agence Nationale de la Recherche (2010BLAN1616 to N.R. and J.C.)

REFERENCES

(1) Tamarit, J.; Belli, G.; Cabiscol, E.; Herrero, E.; Ros, J. *J. Biol. Chem.* **2003**, *278*, 25745.
(2) Johansson, C.; Roos, A. K.; Montano, S. J.; Sengupta, R.; Filippakopoulos, P.; Guo, K.; von, D. F.; Holmgren, A.; Oppermann, U.; Kavanagh, K. L. *Biochem. J.* **2011**, *433*, 303.
(3) Zaffagnini, M.; Michelet, L.; Massot, V.; Trost, P.; Lemaire, S. D. *J. Biol. Chem.* **2008**, *283*, 8868.
(4) Fernandes, A. P.; Fladvad, M.; Berndt, C.; Andresen, C.; Lillig, C. H.; Neubauer, P.; Sunnerhagen, M.; Holmgren, A.; Vlamis-Gardikas, A. *J. Biol. Chem.* **2005**, *280*, 24544.
(5) Rodríguez-Manzaneque, M. T.; Tamarit, J.; Bellí, G.; Ros, J.; Herrero, E. *Mol. Biol. Cell* **2002**, *13*, 1109.
(6) Mühlenhoff, U.; Gerber, J.; Richhardt, N.; Lill, R. *EMBO J.* **2003**, *22*, 4815.
(7) Bandyopadhyay, S.; Gama, F.; Molina-Navarro, M. M.; Gualberto, J. M.; Claxton, R.; Naik, S. G.; Huynh, B. H.; Herrero, E.; Jacquot, J.-P.; Johnson, M. K.; Rouhier, N. *EMBO J.* **2008**, *27*, 1122.
(8) Shakamuri, P.; Zhang, B.; Johnson, M. K. *J. Am. Chem. Soc.* **2012**, *134*, 15213.
(9) Vilella, F.; Alves, R.; Rodriguez-Manzaneque, M. T.; Belli, G.; Swaminathan, S.; Sunnerhagen, P.; Herrero, E. *Comp. Funct. Genomics* **2004**, *5*, 328.
(10) Uzarska, M. A.; Dutkiewicz, R.; Freibert, S. A.; Lill, R.; Muhlenhoff, U. *Mol. Biol. Cell* **2013**, *24*, 1830.
(11) Rodríguez-Manzaneque, M. T.; Ros, J.; Cabrito, I.; Sorribas, A.; Herrero, E. *Mol. Cell. Biol.* **1999**, *19*, 8180.
(12) Wingert, R. A.; Galloway, J. L.; Barut, B.; Foott, H.; Fraenkel, P.; Axe, J. L.; Weber, G. J.; Dooley, K.; Davidson, A. J.; Schmidt, B.; Paw, B. H.; Shaw, G. C. *Nature* **2005**, *436*, 1035.
(13) Molina-Navarro, M. M.; Casas, C.; Piedrafita, L.; Bellí, G.; Herrero, E. *FEBS Lett.* **2006**, *580*, 2273.
(14) Belli, G.; Polaina, J.; Tamarit, J.; De La Torre, M. A.; Rodriguez-Manzaneque, M. T.; Ros, J.; Herrero, E. *J. Biol. Chem.* **2002**, *277*, 37590.
(15) Iwema, T.; Picciocchi, A.; Traore, D. A.; Ferrer, J. L.; Chauvat, F.; Jacquamet, L. *Biochemistry* **2009**, *48*, 6041.
(16) Picciocchi, A.; Saguez, C.; Boussac, A.; Cassier-Chauvat, C.; Chauvat, F. *Biochemistry* **2007**, *46*, 15018.
(17) Couturier, J.; Stroher, E.; Albetel, A. N.; Roret, T.; Muthuramalingam, M.; Tarrago, L.; Seidel, T.; Tsan, P.; Jacquot, J. P.; Johnson, M. K.; Dietz, K. J.; Didierjean, C.; Rouhier, N. *J. Biol. Chem.* **2011**, *286*, 27515.
(18) Fish, W. W. *Meth. Enzymol.* **1988**, *158*, 357.
(19) Outten, C. E.; Culotta, V. C. *J. Biol. Chem.* **2004**, *279*, 7785.
(20) Cuozzo, J. W.; Kaiser, C. A. *Nat. Chem. Biol.* **1999**, *1*, 130.
(21) Cosper, M. M.; Krebs, B.; Hernandez, H.; Jameson, G.; Eidsness, M. K.; Huynh, B. H.; Johnson, M. K. *Biochemistry* **2004**, *43*, 2007.
(22) Neese, F.; Solomon, E. I. *Inorg. Chem.* **1999**, *38*, 1847.
(23) Ravi, N.; Bollinger, J. M.; Huynh, B. H.; Edmondson, D. E.; Stubbe, J. *J. Am. Chem. Soc.* **1994**, *116*, 8007.
(24) Unciuleac, M.-C.; Chandramouli, K.; Naik, S.; Mayer, S.; Huynh, B. H.; Johnson, M. K.; Dean, D. R. *Biochemistry* **2007**, *46*, 6812.
(25) Kennedy, M. C.; Beinert, H. *J. Biol. Chem.* **1988**, *263*, 8194.
(26) Bandyopadhyay, S.; Naik, S.; O'Carroll, I. P.; Huynh, B. H.; Dean, D. R.; Johnson, M. K.; Dos Santos, P. C. *J. Biol. Chem.* **2008**, *283*, 14092.
(27) Saas, J.; Ziegelbauer, K.; von Haeseler, A.; Fast, B.; Boshart, M. *J. Biol. Chem.* **2005**, *275*, 2745.
(28) Li, H.; Mapolelo, D. T.; Dingra, N. N.; Naik, S. G.; Lees, N. S.; Hoffman, B. M.; Riggs-Gelasco, P. J.; Huynh, B. H.; Johnson, M. K.; Outten, C. E. *Biochemistry* **2009**, *48*, 9569.
(29) Li, H.; Mapolelo, D. T.; Randeniya, S.; Johnson, M. K.; Outten, C. E. *Biochemistry* **2012**, *51*, 1687.
(30) Hagen, K. S.; Watson, A. D.; Holm, R. H. *J. Am. Chem. Soc.* **1983**, *105*, 3905.
(31) Kennedy, M. C.; Kent, T. A.; Emptage, M. H.; Merkle, H.; Beinert, H.; Münck, E. *J. Biol. Chem.* **1984**, *259*, 14463.
(32) Girerd, J.-J.; Papaefthymiou, G. C.; Watson, A. D.; Gamp, E.; Hagen, K. S.; Edelstein, N.; Frankel, R. B.; Holm, R. H. *J. Am. Chem. Soc.* **1984**, *106*, 5941.
(33) Hagen, W. R. *Biomolecular EPR Spectroscopy*; CRC Press: Boca Raton, FL, 2009.
(34) Richards, A. J. M.; Thomson, A. J.; Holm, R. H.; Hagen, K. S. *Spectrochim. Acta* **1990**, *46A*, 987.
(35) Johnson, M. K. In *Physical methods in bioinorganic chemistry. Spectroscopy and magnetism*, Que, L., Jr., Ed.; University Science Books: Sausalito, CA, 2000; p 233.
(36) Han, S.; Czernuszewicz, R. S.; Spiro, T. G. *J. Am. Chem. Soc.* **1989**, *111*, 3496.
(37) Han, S.; Czernuszewicz, R. S.; Kimura, T.; Adams, M. W. W.; Spiro, T. G. *J. Am. Chem. Soc.* **1989**, *111*, 3505.
(38) Fu, W.; Drozdzewski, P. M.; Davies, M. D.; Sligar, S. G.; Johnson, M. K. *J. Biol. Chem.* **1992**, *267*, 15502.
(39) Agar, J. N.; Krebs, B.; Frazzon, J.; Huynh, B. H.; Dean, D. R.; Johnson, M. K. *Biochemistry* **2000**, *39*, 7856.
(40) Chandramouli, K.; Unciuleac, M.-C.; Naik, S.; Dean, D. R.; Huynh, B. H.; Johnson, M. K. *Biochemistry* **2007**, *46*, 6804.
(41) Mapolelo, D. T.; Zhang, B.; Naik, S. G.; Huynh, B. H.; Johnson, M. K. *Biochemistry* **2012**, *51*, 8071.
(42) Khoroshilova, N.; Popescu, C.; Münck, E.; Beinert, H.; Kiley, P. J. *Proc. Natl. Acad. Sci. U.S.A.* **1997**, *94*, 6087.
(43) Beinert, H.; Holm, R. H.; Münck, E. *Science* **1997**, *277*, 653.
(44) Czernuszewicz, R. S.; Macor, K. A.; Johnson, M. K.; Gewirth, A.; Spiro, T. G. *J. Am. Chem. Soc.* **1987**, *109*, 7178.
(45) Conover, R. C.; Kowal, A. T.; Fu, W.; Park, J.-B.; Aono, S.; Adams, M. W. W.; Johnson, M. K. *J. Biol. Chem.* **1990**, *265*, 8533.
(46) Brereton, P. S.; Duderstadt, R. E.; Staples, C. R.; Johnson, M. K.; Adams, M. W. W. *Biochemistry* **1999**, *38*, 10594.
(47) Rouhier, N.; Couturier, J.; Johnson, M. K.; Jacquot, J. P. *Trends Biochem. Sci.* **2010**, *35*, 43.
(48) Yeung, N.; Gold, B.; Liu, N. L.; Prathapam, R.; Sterling, H. J.; Willams, E. R.; Butland, G. *Biochemistry* **2011**, *50*, 8957.
(49) Gailer, J.; George, G. N.; Pickering, I. J.; Prince, R. C.; Kohlhepp, P.; Zhang, D.; Walker, F. A.; Winzerling, J. J. *J. Am. Chem. Soc.* **2001**, *123*, 10121.
(50) Krebs, C.; Henshaw, T. F.; Cheek, J.; Huynh, B. H.; Broderick, J. B. *J. Am. Chem. Soc.* **2000**, *122*, 12497.
(51) Ye, H.; Jeong, S. Y.; Ghosh, M. C.; Kovtunovych, G.; Silvestri, L.; Ortillo, D.; Uchida, N.; Tisdale, J.; Camaschella, C.; Rouault, T. A. *J. Clin. Invest.* **2010**, *120*, 1749.
(52) Haunhorst, P.; Berndt, C.; Eitner, S.; Godoy, J. R.; Lillig, C. H. *Biochem. Biophys. Res. Commun.* **2010**, *394*, 372.
(53) Subramanian, S. Ph.D. Dissertation, University of Georgia, 2010.
(54) Zhang, B. Ph.D. Dissertation, University of Georgia, 2013.
(55) Leal, S. S.; Teixeira, M.; Gomes, C. M. *J. Biol. Inorg. Chem.* **2004**, *9*, 987.
(56) Jones, K.; Gomes, C. M.; Huber, H.; Teixeira, M.; Wittung-Stafshede, P. *J. Biol. Inorg. Chem.* **2002**, *7*, 357.
(57) Griffin, S.; Higgins, C. L.; Soulimane, T.; Wittung-Stafshede, P. *Eur. J. Biochem.* **2003**, *270*, 4736.
(58) Higgins, C. L.; Wittung-Stafshede, P. *Arch. Biochem. Biophys.* **2004**, *427*, 154.
(59) Sipos, K.; Lange, H.; Fekete, Z.; Ullmann, P.; Lill, R.; Kispal, G. *J. Biol. Chem.* **2002**, *277*, 26944.
(60) Li, H.; Outten, C. E. *Biochemistry* **2012**, *51*, 4377.
(61) Mühlenhoff, U.; Molik, S.; Godoy, J. R.; Uzarska, M. A.; Richter, N.; Seubert, A.; Zhang, Y.; Stubbe, J.; Pierrel, F.; Herrero, E.; Lillig, C. H.; Lill, R. *Cell Metab.* **2010**, *12*, 373.